BCAL Segmentation and Reconstruction

David Lawrence

1 $\theta = 90^\circ$ clean showers

Plots 2-4 were generated using the particle gun to shoot photons at 90 degrees into the center of the BCAL. The particles were shot from the beam line and passed between FDC packages, avoiding much of their material. In addition, the dark pulses, energy smearing due to sampling, time smearing, and applied threshold were disabled in *mcsmear* to leave relatively clean showers. The energy range for these events was 160-680MeV.

Below are definitions of a few of the energy terms found on the plots below.

E_{recon} Reconstructed energy as read from DBCALShower::E. In the case of KLOE code, this includes the energy correction function (see fig. 6).

E_{raw} Sum of energy from each cell $before$ the correction function is applied. For cases where the smearing, dark pulses and fADC level thresholds are disabled, this will correspond the exact energy deposited in the calorimeter for those cells included in the cluster. This is read from DBCALShower::E_raw.

$\Sigma E_{truthhits}$ Sum of energy from all DBCALTruthCell objects. For the events in this study, a single incident particle exists so all energy must come from it. Many events have splitoff particles that travel to parts of the BCAL where the energy is deposited ($\sim 1 - 2MeV$). The splitoffs are included here, but that energy will not be included in the reconstructed values.

E_{gen} The generated energy given to the incident photon in GEANT.

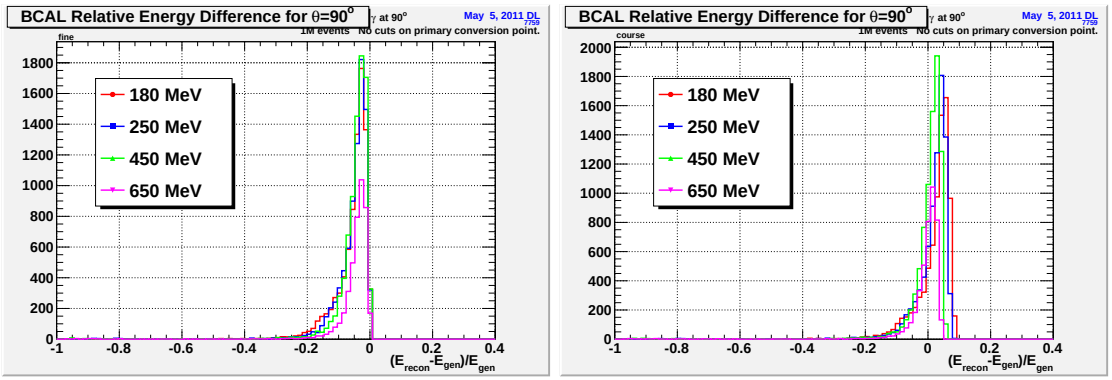

Figure 1: Relative energy difference (Normalized to generated energy) for fine(left) and course(right) segmentation schemes. See fig. 2 for the un-normalized distributions.

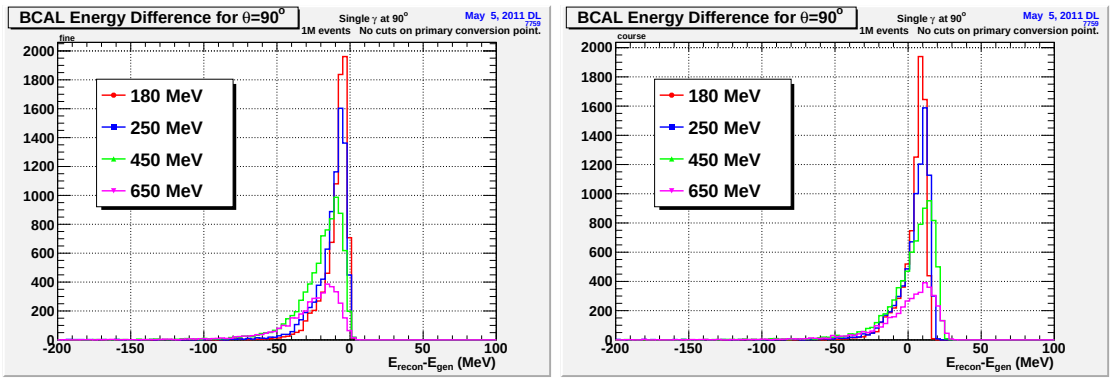

Figure 2: Difference between reconstructed and generated energy for 90^o photons incident on the center of the BCAL in z. No dark pulses, energy smearing, time smearing, or fADC level thresholds were included in the smearing of the simulated data. The energy correction functions (see fig. 6) were still applied however, which assumed these effects were included.

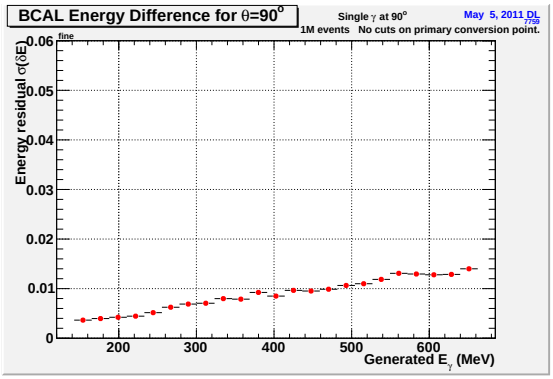

Figure 3: Width of distributions such as those shown in the plot on the left in fig 2. The values were the σs resulting from Gaussian fits (not necessarily the best shape).

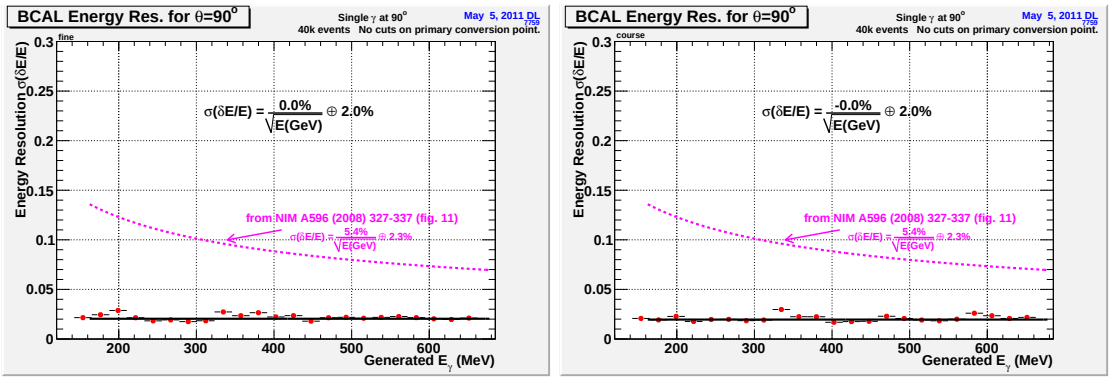

Figure 4: Intrinsic energy resolution of GEANT generated data. For these plots, the dark pulses, energy smearing (mcsmear), time smearing (mcsmear) and fADC level thresholds were disabled. The resulting width is due to energy leakage (see fig. 1).

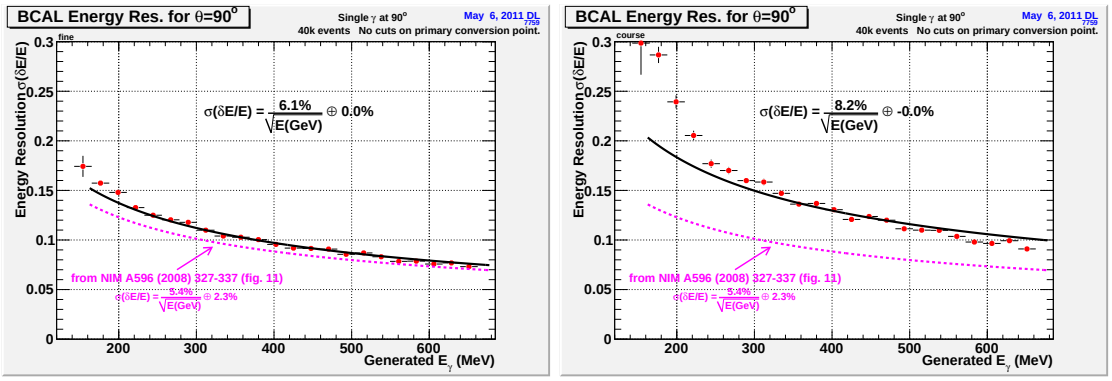

Figure 5: Energy resolution obtained when using full simulation (including all dark pulses and energy smearing features). Reconstruction is done using the KLOE code.

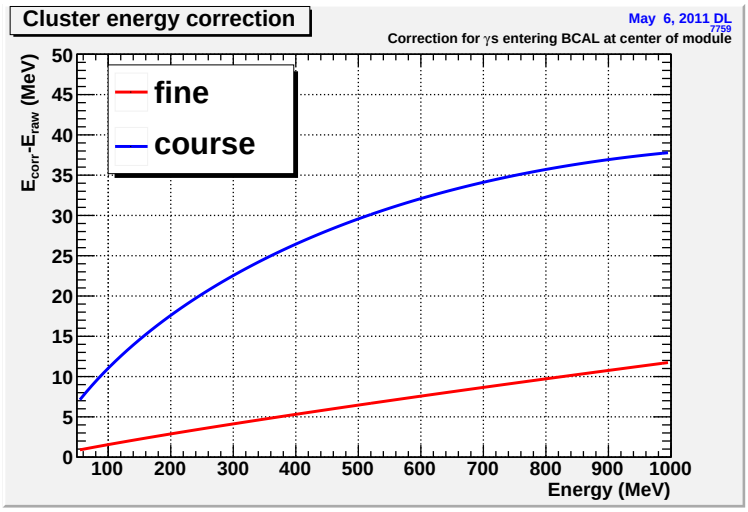

Figure 6: Energy correction at 90^o as a function of energy as applied in the KLOE reconstruction code. The curves shown here are for showers entering at the center of the BCAL.

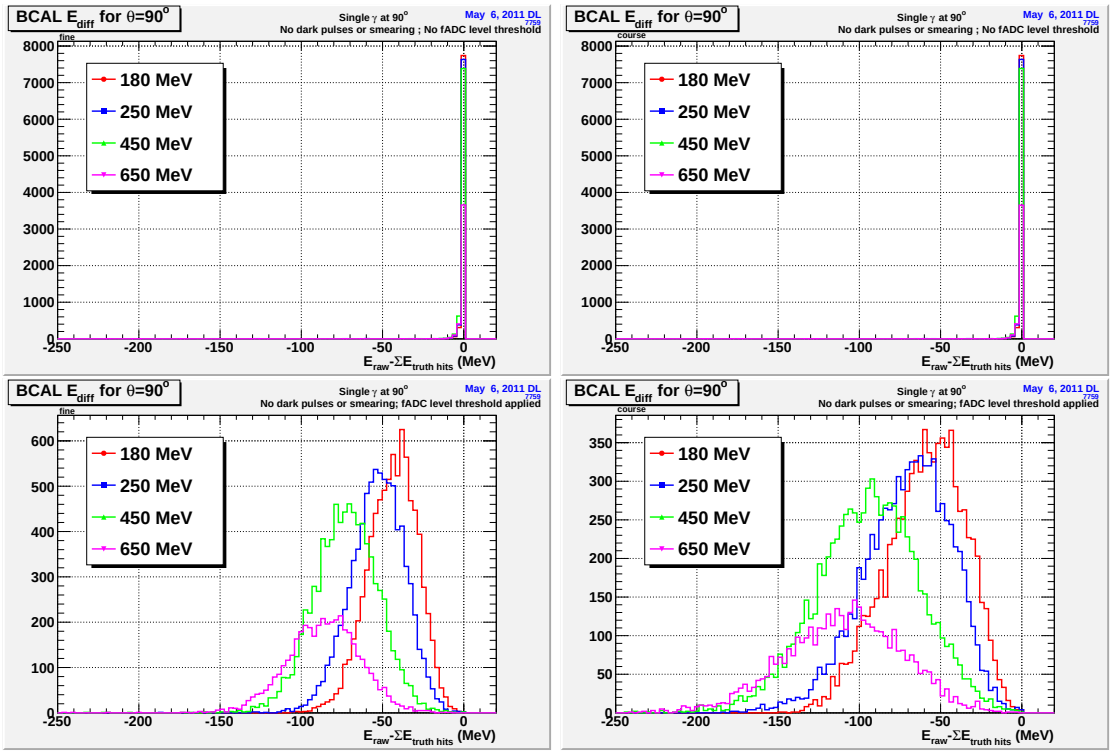

Figure 7: Energy loss with(top) and without(bottom) the fADC level threshold applied. The fine segmentation scheme is shown in the plots on the left while the course segmentation is on the right. The small tail to the left of the top plots is due to energy leakage (mainly out the back for 90^o incident particles.

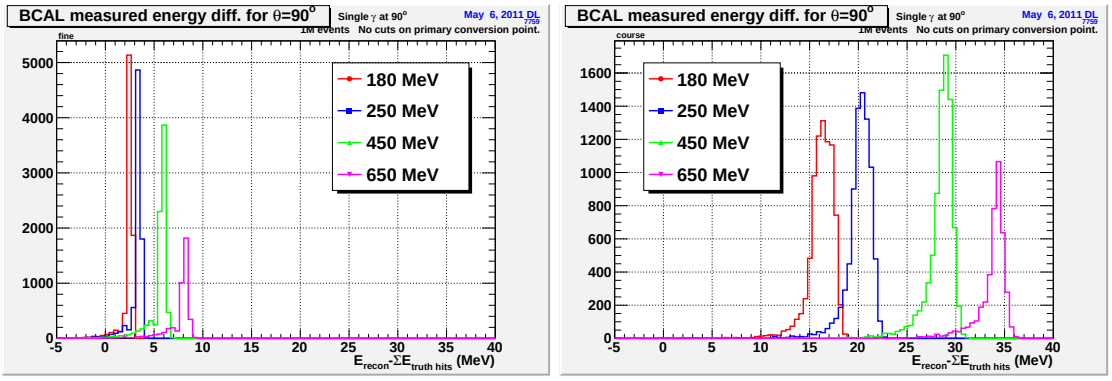

Figure 8: Difference between reconstructed energy and sum of energy from all cells hit. The sum comes from summing over all DBCALTruthCell objects (which are copies of the information in HDDM in $barrelEMcal- > bcalCell- > bcalHit$). These are for 90^o incident photons in the center of the BCAL. Dark pulses, energy smearing (mcsmear), time smearing (mcsmear) and fADC level thresholds were disabled. The fine segmentation scheme is on the left while the course scheme is on the right. The deviation from zero is due to the correction factor (fig. 6) being applied to data for which the sources of error that lead to the corrections have been removed.

2 Full simulation/reconstruction

Plots 10-18 were generated using the standard simulation which includes dark pulses, thresholds, and smearing of both timing and energy values.

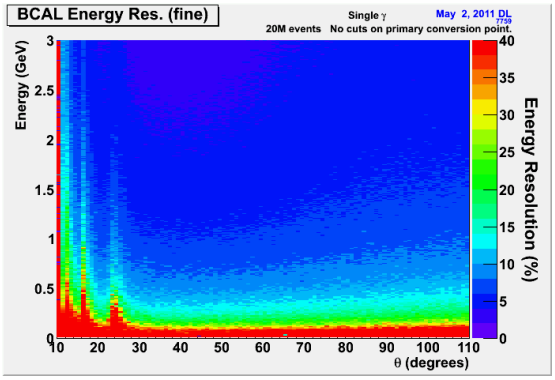

Figure 9: Energy resolution (relative) as a function of generated energy and generated polar angle θ. These are results from Gaussian fits to the relative energy difference.

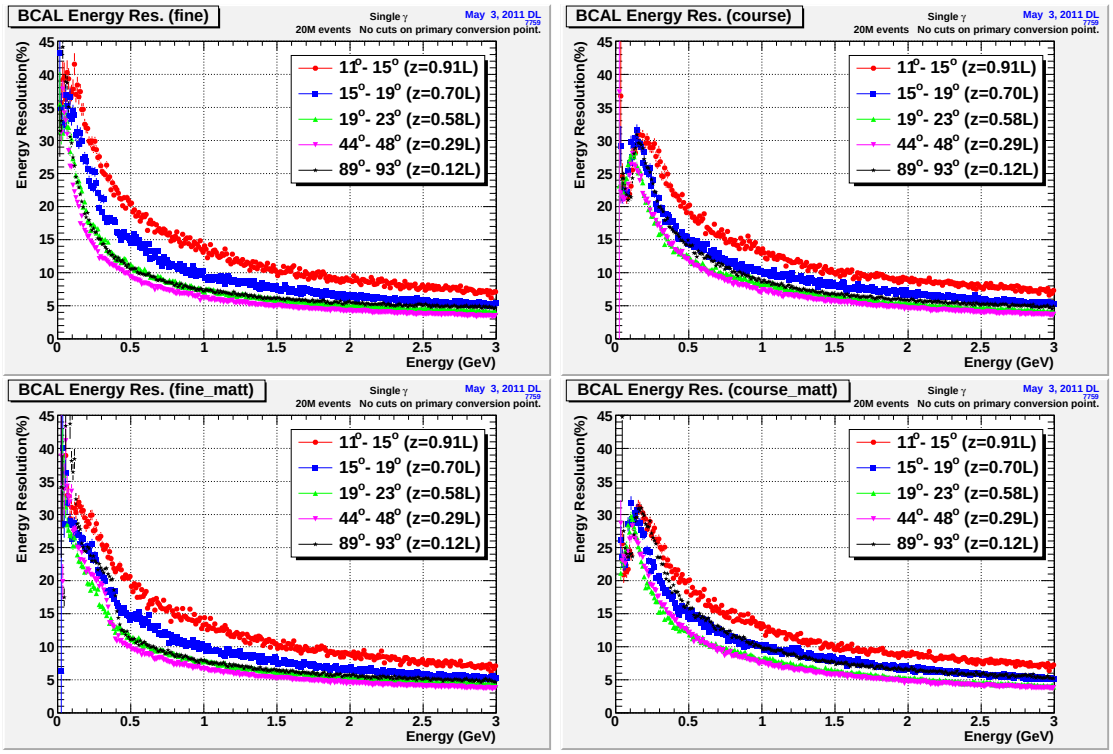

Figure 10: Energy resolution as a function of energy for various angular ranges. Shown are the KLOE algorithm (top) and the Indiana algorithm (bottom) for the fine segmentation scheme (left) and course segmentation scheme (right). These are obtained from Gaussian fits to the relative energy distribution for individual bins in figure 9.

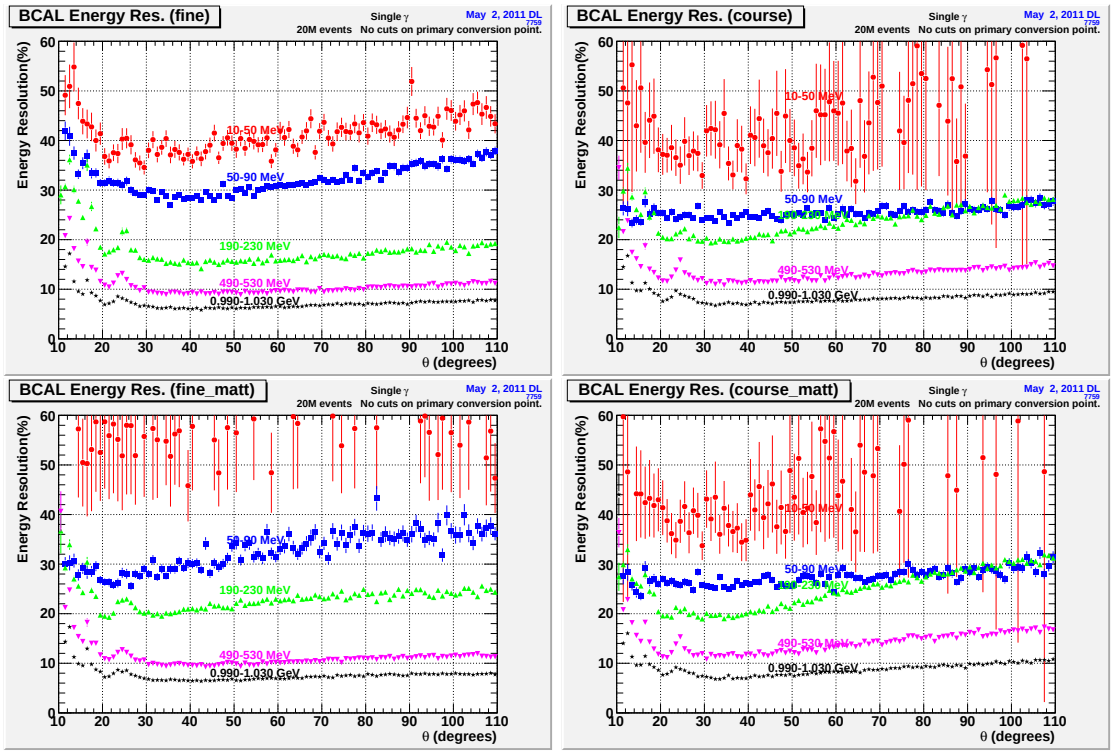

Figure 11: Energy resolution as a function of θ for various energy ranges. Shown are the KLOE algorithm (top) and the Indiana algorithm (bottom) for the fine segmentation scheme (left) and course segmentation scheme (right). These are obtained from Gaussian fits to the relative energy distribution for individual bins in figure 9.

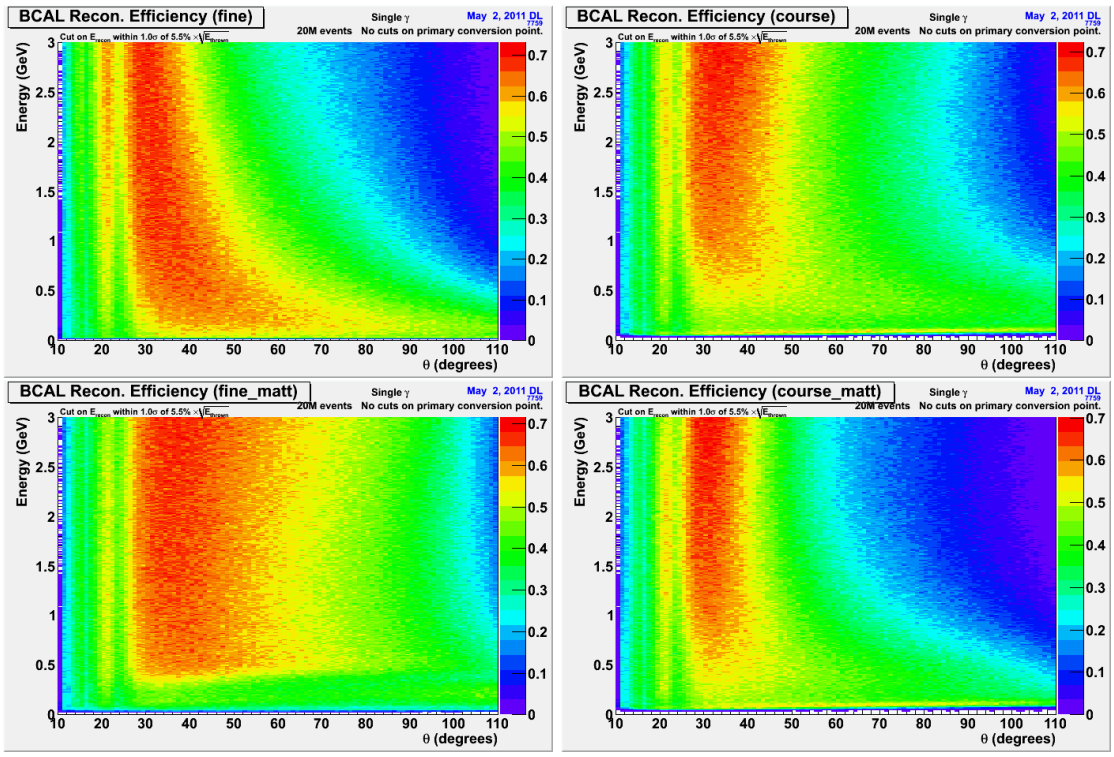

Figure 12: Efficiency for 1σ cut where $\sigma = 5.5\%/\sqrt{E}$.

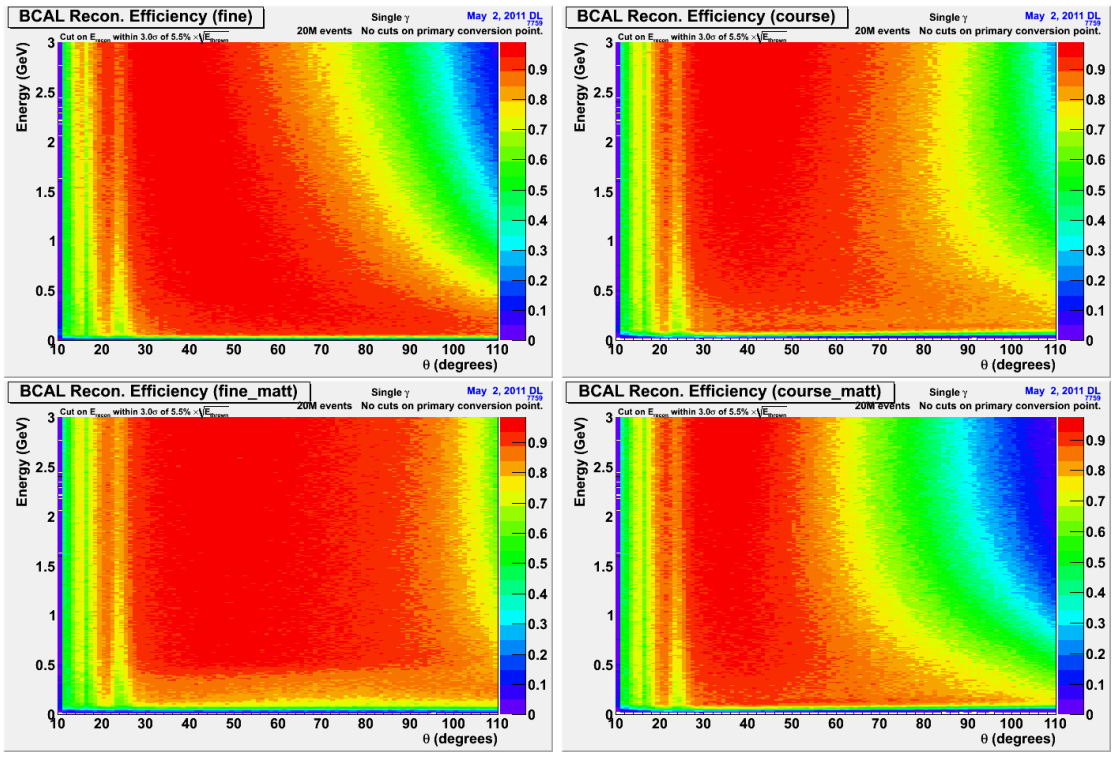

Figure 13: Efficiency for 3σ cut where $\sigma = 5.5\%/\sqrt{E}$.

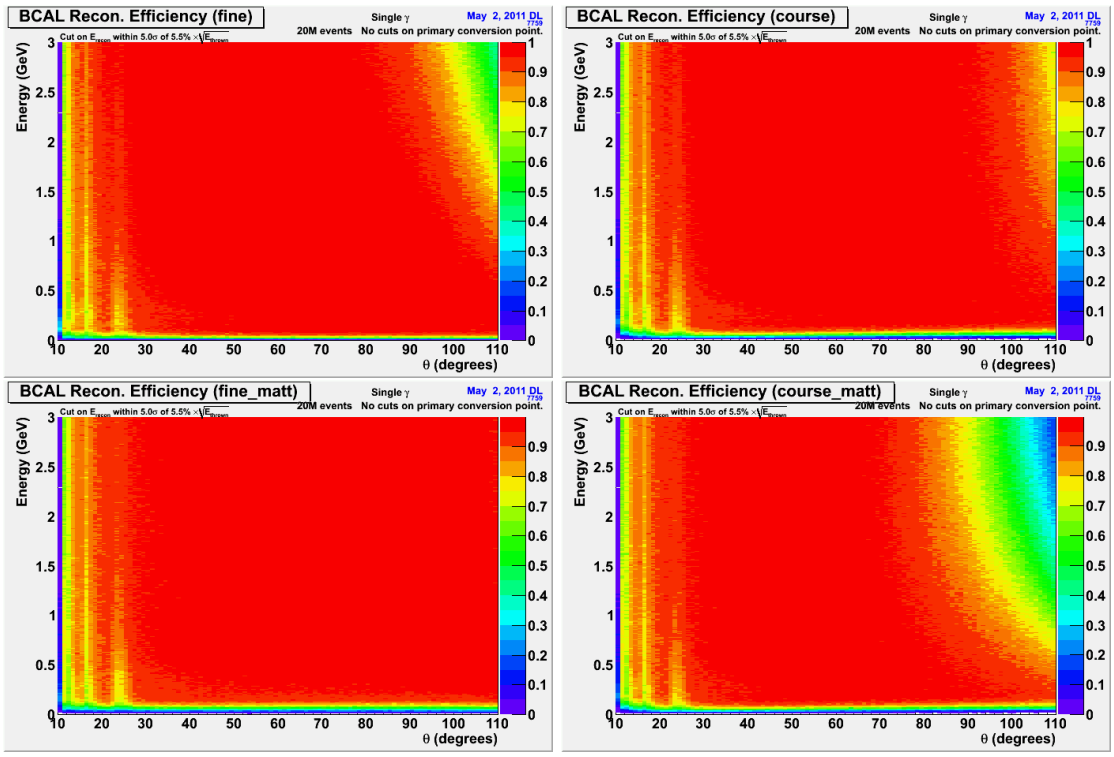

Figure 14: Efficiency for 5σ cut where $\sigma = 5.5\%/\sqrt{E}$.

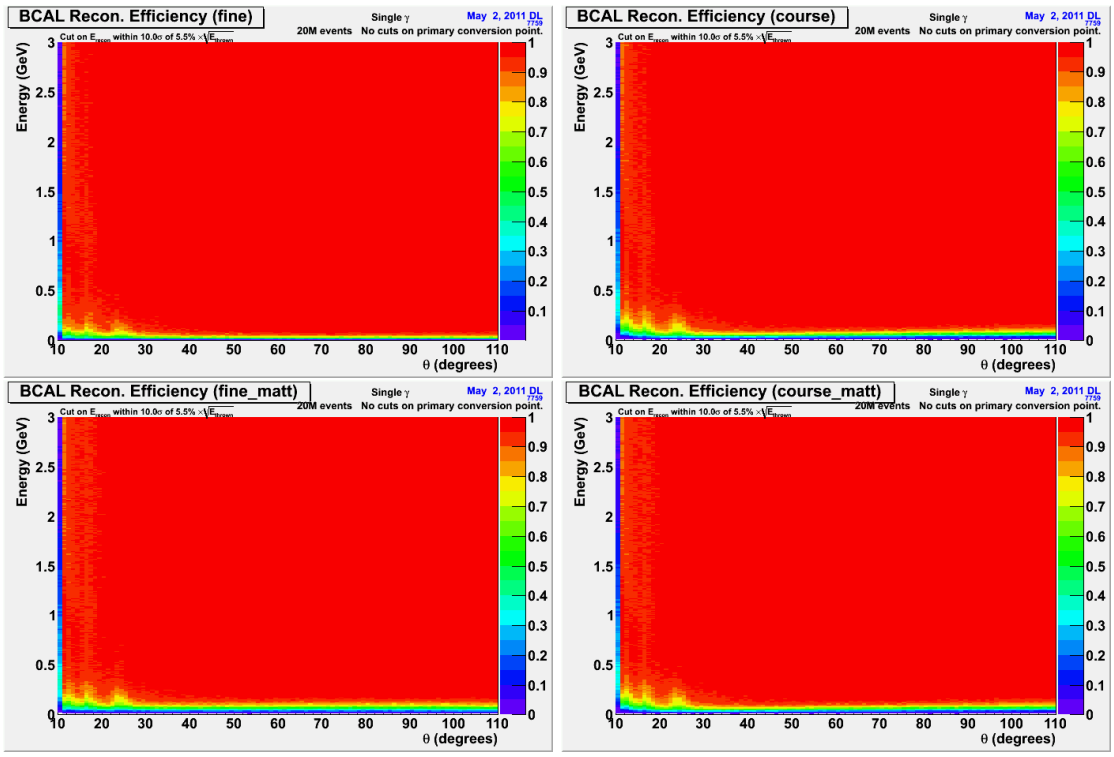

Figure 15: Efficiency for 10σ cut where $\sigma = 5.5\%/\sqrt{E}$.

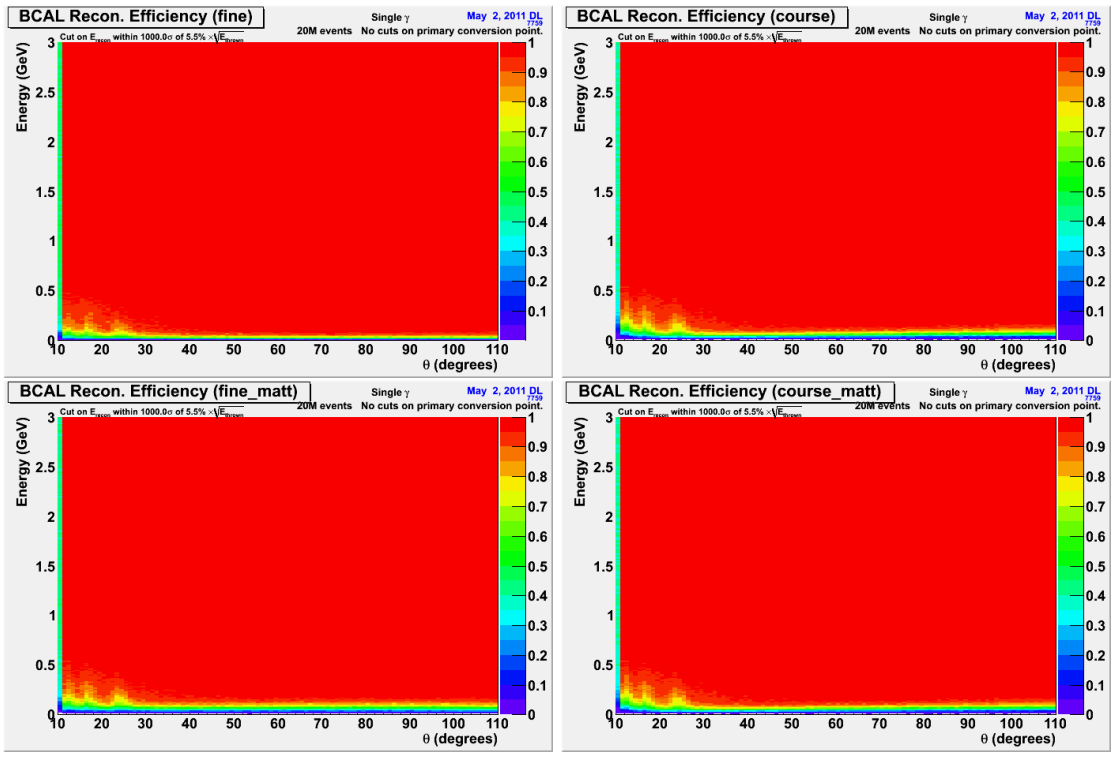

Figure 16: Efficiency for 1000σ cut where $\sigma = 5.5\%/\sqrt{E}$.

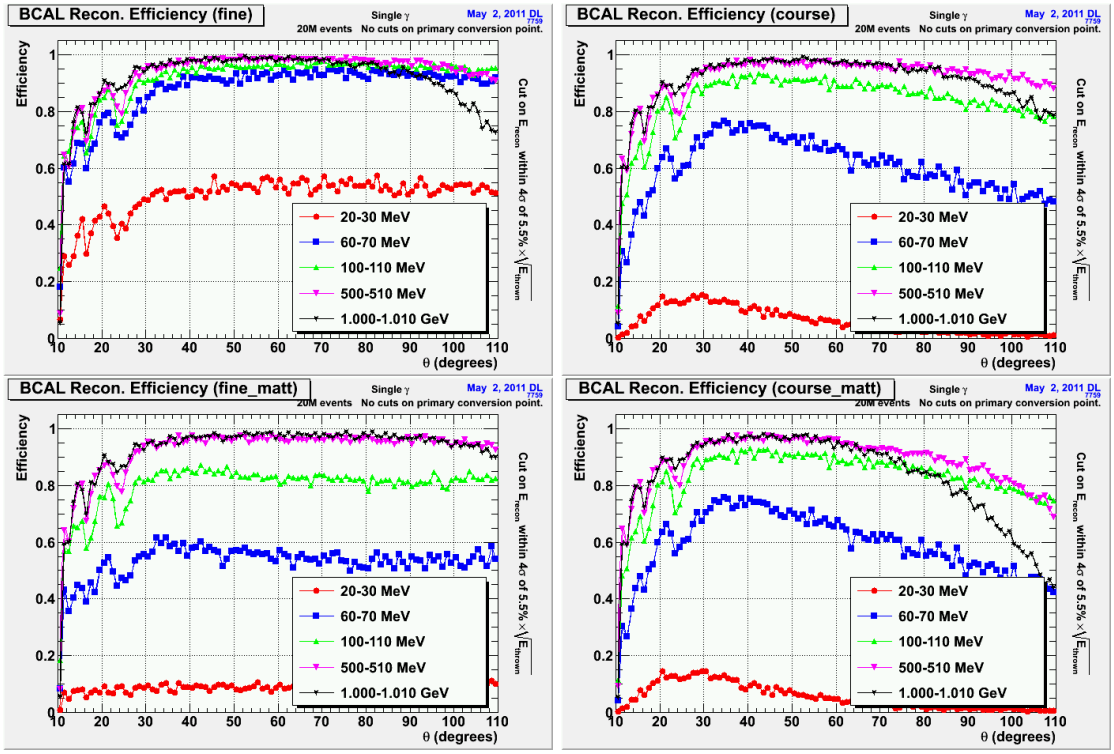

Figure 17: Reconstruction efficiency (projections) from 4σ cut for both reconstruction algorithms applied to both segmentation schemes. Shown are the KLOE algorithm (top) and the Indiana algorithm (bottom) for the fine segmentation scheme (left) and course segmentation scheme (right).

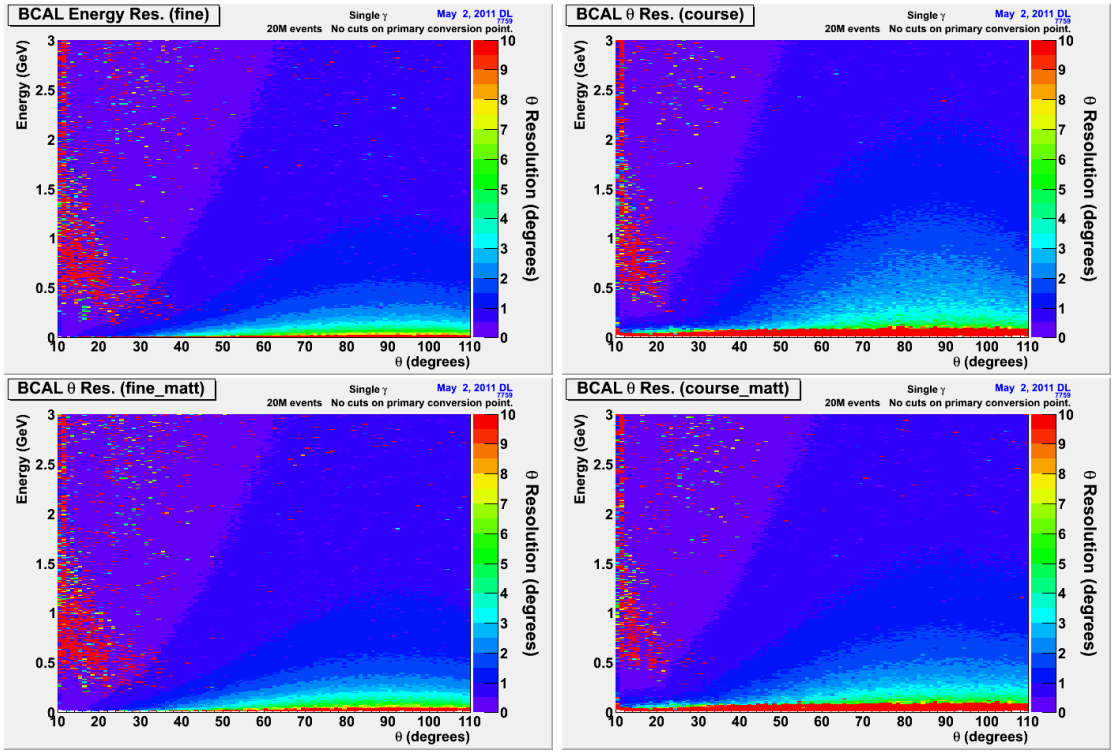

Figure 18: θ angular resolution for both reconstruction algorithms applied to both segmentation schemes.

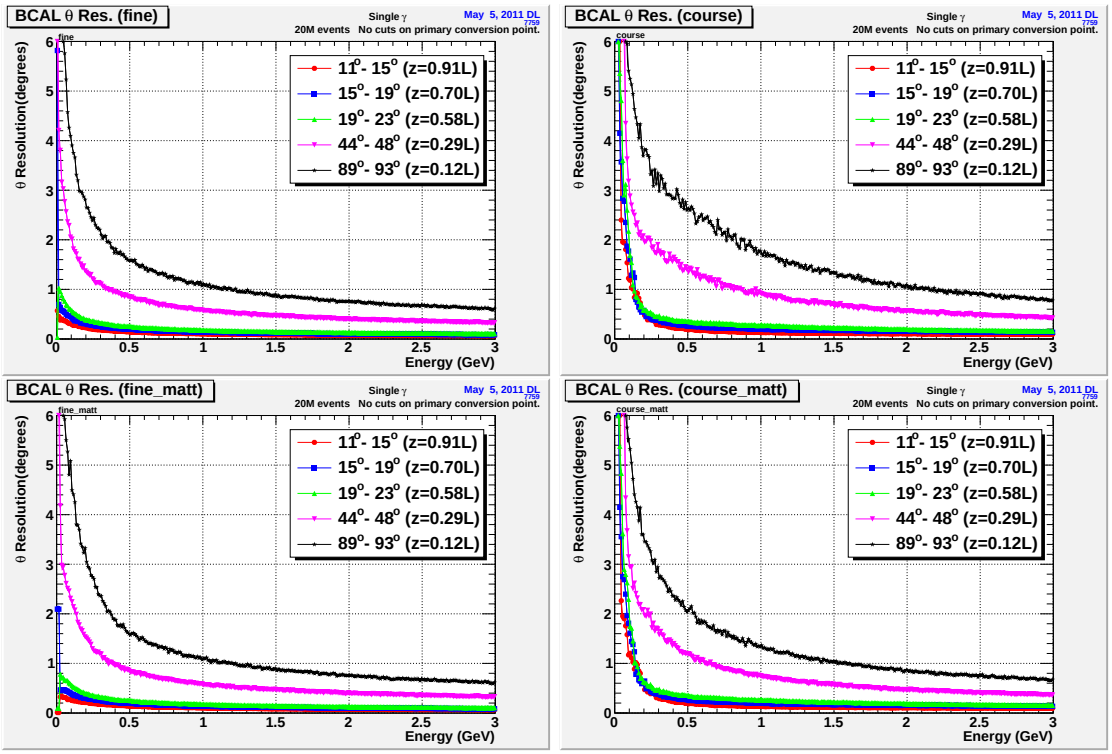

Figure 19: θ angular resolution (projections) for both reconstruction algorithms applied to both segmentation schemes.